ACS OMEGA

http://pubs.acs.org/journal/acsodf

Article

Latent, Cross-Linkable Triazole Platform on a Carbon Fiber Surface for Enhancing Interfacial Cross-Linking within Carbon Fiber/Epoxy Composites

Jae-Ho Shin, Gi-Yeon Han, and Hyun-Joong Kim*

Cite This: https://doi.org/10.1021/acsomega.2c00045

Read Online

ACCESS | Metrics & More | Article Recommendations | Supporting Information

ABSTRACT: A long-running need in carbon fiber composite production is to ameliorate interfacial adhesion between the polymer and carbon fibers. Here, we present a convenient and feasible strategy for controlling the carbon fiber's surface in a continuous process: syntheses of click-modified silanes via copper(I)-catalyzed azide−alkyne cycloaddition reaction and grafting them onto fiber surfaces which prepare a latent curable platform under mild processes without postmodification. As 1,2,3-triazole moieties from the click reaction were added to the epoxy/dicyandiamide system, they triggered additional reactions in the later conversion stage; approximately, a 20% increase in the total reaction enthalpy compared to the system with no additives was obtained. We expected the enhanced cross-linking between the surface and matrix to expand the interfacial area, leading to reinforcements on interfacial adhesion and stress-transfer abilities within composites. The merit of the approach is well-demonstrated by conductive atomic force microscopy, showing that the interphase can be extended up to 6-fold when the triazole platform acts as curatives and serve as bridges after the epoxy cure. Consequently, the composite's interfacial shear strength and interlaminar shear strength were increased up to 78 and 72%, respectively. This work affords a reactive platform where a custom-tailored fiber/matrix interface can be designed by virtue of versatility in clickable reactants.

1. INTRODUCTION

On the threshold of ground-breaking changes in the transportation industry nowadays, much more stringent regulations regarding weight reduction and fuel efficiency and multipronged energy-saving strategies are expected in the field of material engineering.[1] As a promising alternative to conventional load-bearing materials like heavy metals, carbon fiber reinforced polymers (CFRPs) are now taking the lead in the competition among lightweight composites,[2] demonstrating structural versatility in processing and supreme mechanical performance and chemical tolerance. Nevertheless, due to the chemical inertness of the carbon fiber (CF)—the stress-bearing core component in CFRP and the consequential weak interfacial adhesion within multicomponents—the composite could not fully function its maximum performance. The composite's interphase is vulnerable to an external shear and pull-off (perpendicular to the direction of CF layers) stress, resulting in material breakage in multiple dimensions from interfacial failure at the CF surface[3] to delamination of exterior-interior prepreg layers.[4] It is well established that the chemical interactions and mechanical interlocking within the interphase/interface between the CF and resin polymer dictate the interfacial adhesion properties of the composite.[5] Hence, the development of technologies that design the CF/matrix interface and improve both the chemical affinity and physical effects are key to remedy the CFRP's shortcoming and adopt it as a practical transportation material.

With outgrowing interest in CF interface engineering, there have been many approaches to design the interface in accordance with their applications. Of particular interest in this paper is the grafting of coupling agents to the CF surface to tailor interfacial characteristics and impart some special functions. For that, fabrication of a reactive molecular platform on the aloof surface is always an effective tactic, irrespective of the substrate type for further functionalization.[6,7] Several researchers preinstalled reactive groups on various target substrates and utilized them in the epoxy cure procedure so that the curable functionalities such as amine,[8,9] thiol,[10] hydroxy,[11] and imidazole[12] could contribute to the epoxy ring−opening reaction, reinforcing the resultant filler-matrix interface. However, considering the filaments' storage and

Received: January 4, 2022
Accepted: March 22, 2022

processing conditions, the curatives need latency against external stimuli to prevent unwanted conversion and provide sufficient room for controlling B-stage prepreg. For example, with imidazole as the most abundant latent cure agent, its reactivity under mild conditions makes it a viable candidate to function as an interface linker. Using heat as a trigger, activation by epoxide forms the 1:1 O^- adduct or 2:1 O^-/OH adduct[13] inducing a cross-linking effect between epoxide and other reactants in the system. However, several drawbacks, including low kick-off temperature and short shelf-life, compromise its use in practical applications.

With a perspective on molecular structure, a 1,2,3-triazole ring, from the so-called copper-catalyzed azide−alkyne cycloaddition reaction (CuAAC), should be effective as a curative in lieu of imidazole, thanks to the two basic pyridine-type (−N═) nitrogen atoms and one tertiary amine (−N−) assembled within the five-membered ring. This supports a strong potential for reactivity toward the epoxide. What differentiates the click reaction product from imidazoles is the unparalleled versatility in selecting the starting ingredients (e.g., species of azides and alkynes) and derivatives with various end groups. This can tailor curable reactivity suitable for bespoke applications. Unsurprisingly, the deposition of clickable groups (azide or acetylenes) on a substrate gained much attention, given the unique characteristics of a "click" type reaction: high selectivity, low byproduct formation, and mild reaction condition.[14] This enables quantitative conversion and high yield of building blocks onto a surface. Servinis et al. employed an electrochemical deposition method to tether a small molecule with an alkynyl end group to a CF surface and added azides afterward.[15] Similarly, Randall et al. preinstalled a phenylacetylene (PA) group on the CF and attached polyethylene oxide with an azide end group and conducted the CuAAC click reaction in the DMF medium.[16] They both successfully grafted the target molecules and achieved very high gains in interfacial shear strength (IFSS) in click-functionalized CF specimens and ascribed the credit to the mechanical interlocking effects of the surface-grafted molecules based on molecular modeling and pull-out simulations. In addition to these studies, it would be beneficial to elucidate the role of the click building blocks and possible reactions at the CF/matrix interface during the curing process. Our aim herein is to expand this methodology with due consideration to latent cure properties of triazoles at the CF surface and its impact on reinforcing CF/matrix interfacial adhesion. To this end, we propose a one-step "graft-to" of the click reacted silane coupling agents (SCAs) on CF as a feasible strategy to induce cross-linking via latent building block activations at elevated temperatures. This may permit the reinforcement of the interfacial adhesion between the epoxy matrix and CF.

We started our studies by preparing azido-terminated silane via S_{N_2} nucleophilic substitution and converting the product via the CuAAC reaction to synthesize triazole-centered SCA with two different pendants for comparison (Figure 1). Once the SCA was prepared, the "graft-to" approach underwent oxidation of the CF surface within an hour in the ethanol/water medium (Figure 2). In this way, a shorter reaction time would be expected than the postmodification method on the surface-bound azide or acetylene groups.[7,17] Then, we tested the potency of latent curability for all SCAs with different end functionalities, including amine, imidazoline, and triazoles. We seek to explore how each surface treatment affects the formation of the CF/epoxy resin interphase and their interfacial adhesion performance in the composite for the viable candidates.

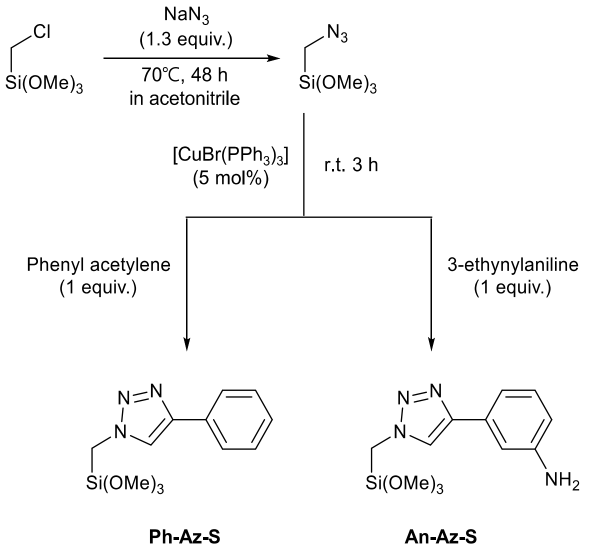

Figure 1. Synthetic pathway to prepare Ph-Az-S and An-Az-S SCA via (top) S_{N_2} substitution reaction and (bottom) the followed CuAAC click reaction.

2. RESULTS AND DISCUSSION

2.1. Characterization on CF Surfaces.

The pristine and oxidized fibers were collected as the base material for analysis. When the "graft-to" process was completed, the functionalized CF was also collected and named after the SCA used in each run. The type of SCA was correlated with the change in surface characteristics. First, in advance of other surface characterizations, we needed to confirm the surface homogeneity of the functionalized CF. The FE-SEM images of $CF_{Pristine}$, CF_{Ox} (oxidized), CF_{APTMS}, CF_{IZPS}, $CF_{Ph\text{-}Az\text{-}S}$, and $CF_{An\text{-}Az\text{-}S}$ were photographed, and the representative images are provided in Figure S5. The characteristic grooves along the fiber, which originated from the polyacrylonitrile (PAN) wet-spinning process,[18] were consistently observed in all CFs. While the $CF_{Pristine}$ showed a relatively smooth surface with a few shallow striations, the grooves on the CF_{Ox} were deepened in the wake of surface oxidation and etching (Figure S5b: CF surface morphology before and after silane functionalization). The surface of functionalized CF, on the other hand, revealed a top coat on their surface. The SCA shrouded the carbon fibers forming a self-condensed polysiloxane layer, leading to homogeneous coating, endowing hydrophobicity, and changing the CF's interfacial properties. As a result, the enhanced dispersion for silane-grafted fibers within the epoxy matrix yielded better interaction between them than expected. The water contact angle (WCA) measurements on the pristine and functionalized CFs confirmed the increased hydrophobicity for the "graft-to" functionalized CF (Figure S6: WCA characterization on CF surfaces). As the initial silane dose in a medium increased, the WCA on the functionalized CF's surface increased and approached a steady value after 20 mmol g_{fiber}^{-1} doses, irrespective of the types of SCA, and this dose was adopted hereafter.

We further characterized the chemical state of $CF_{Pristine}$, CF_{Ox}, and the functionalized CF surfaces by XPS analyses and

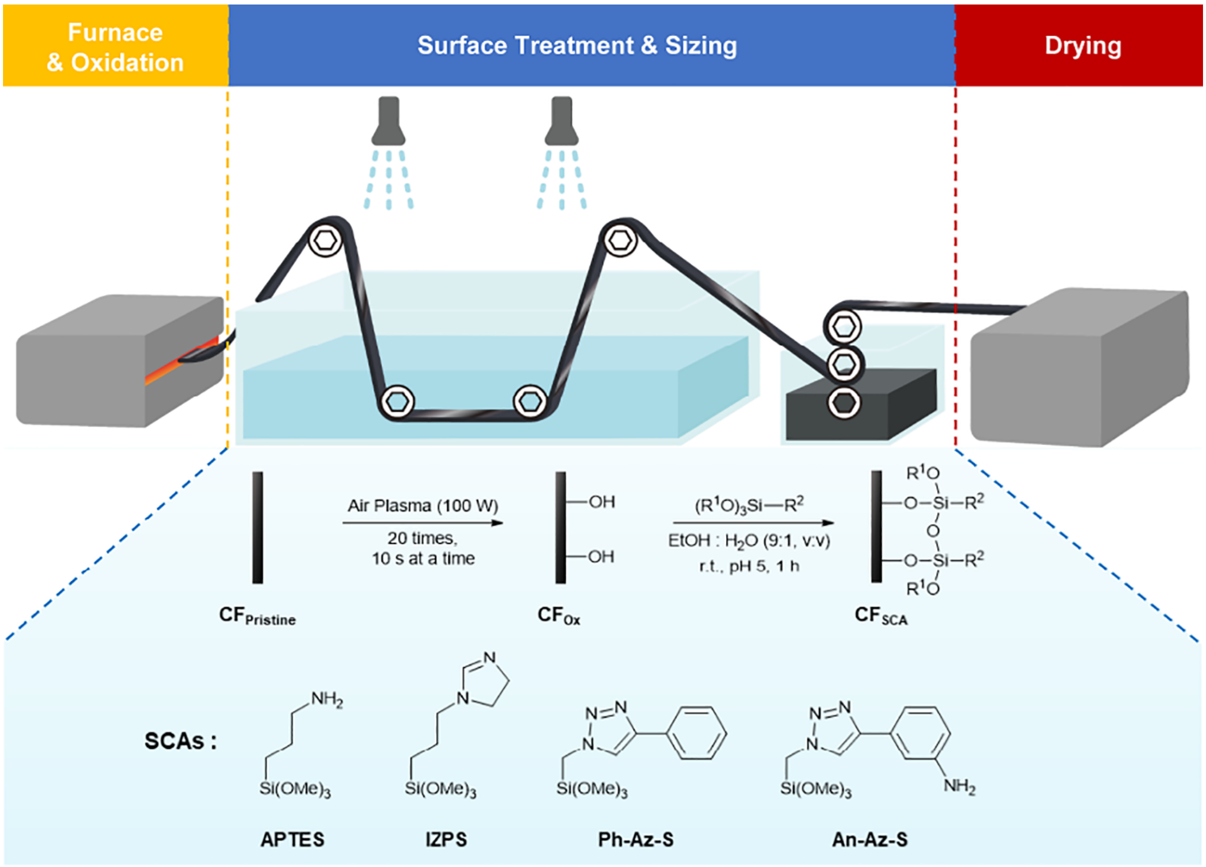

Figure 2. (Top) carbon fiber manufacturing process. (Bottom) installation of four types of SCA on the fiber's surface.

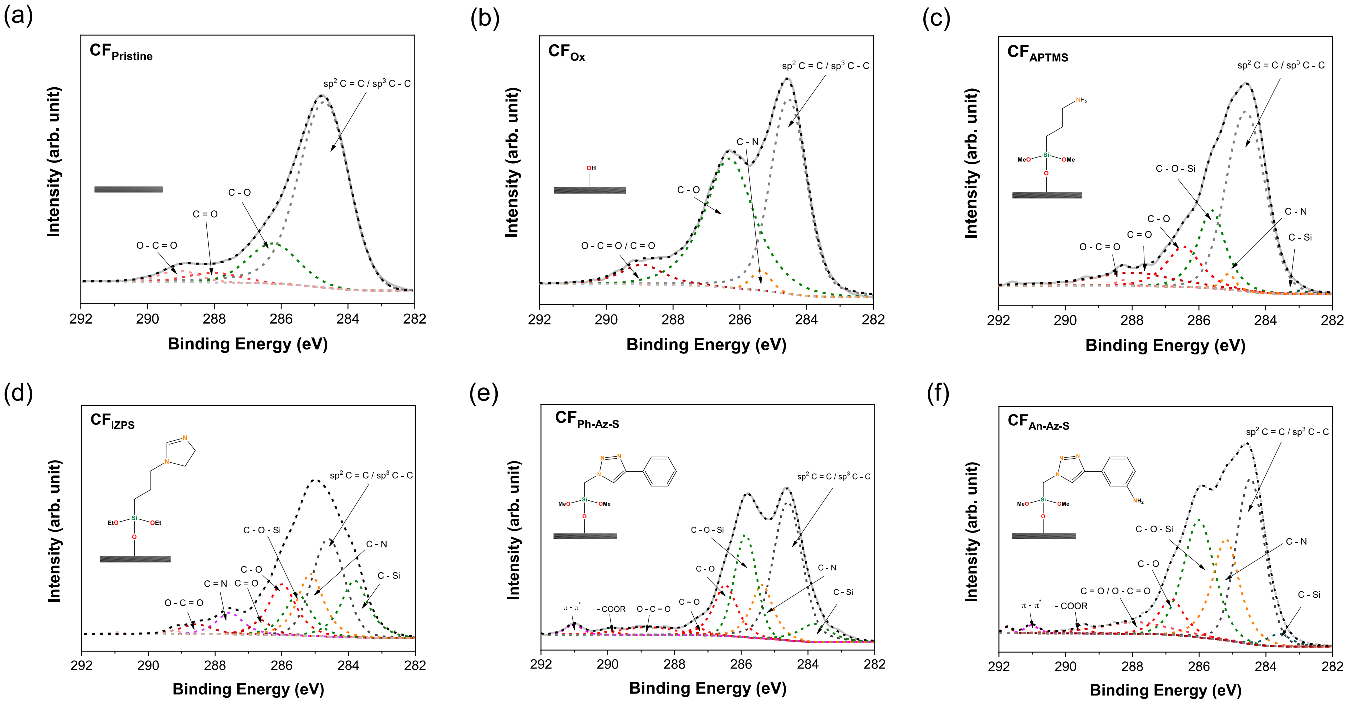

Figure 3. XPS C_{1s} high-resolution spectra for the pristine and functionalized CF. (a) $CF_{Pristine}$, (b) CF_{Ox}, (c) CF_{APTMS}, (d) CF_{IZPS}, (e) $CF_{Ph\text{-}Az\text{-}S}$, and (f) $CF_{An\text{-}Az\text{-}S}$.

determined their atomic concentrations based on integral peak intensities obtained from survey scan C_{1s}, N_{1s}, O_{1s}, and Si_{2p} (Table S1: Elemental analysis on CFs). The relative sensitivity factors used for C, N, O, and Si were 1.0, 1.8, 2.93, and 0.82, respectively, provided by the manufacturer. Each chemical state of CF was determined by its corresponding photoelectron core-level C_{1s} peaks deconvoluted using the peak fitting method (see the Supporting Information). Four broad C_{1s} deconvoluted peaks in $CF_{Pristine}$ in the range of 292−282 eV were yielded (Figure 3a) corresponding to the graphitic carbon (sp^2 C═C bond) with adventitious carbon (sp^3 C−C bonds) (dominant peak, 284.6 eV), alcoholic or ether C−O bonds (286.2 eV), carbonyl C═O bonds (288.0 eV), and carboxyl or ester O−C═O bonds (289.1 eV).[19] Little spectroscopic signatures of nitrogen species were obtained in both the C_{1s} and N_{1s} photoelectron spectra of $CF_{Pristine}$. In CF_{Ox}, a decrement of carbon content and an increment of oxygen content were observed in both the C_{1s} deconvoluted peaks and its elemental composition from the survey spectrum. Meanwhile, the sudden appearance of N_{1s} emission at ∼400 eV is also noticeable due to the exposure of bare CF surface to acridone, naphtyridine, and hydronaphtyridine rings. This may have remained from the production stage[20] or the sputtering of nitrogen radicals or ions during air ionization onto the unstable CF surface.[21]

Grafting the SCA drastically changed the chemical state of each CF surface. For the CF functionalized with SCA, silicon element contents increased from 2% to above 10% based on their elemental composition analysis. In all C_{1s} high-resolution spectra, two new closely related energy peaks appeared, located at 285.5 eV (±0.3 eV) and 283.6 (±0.3 eV), which denote the formation of C−O−Si and C−Si linkages, respectively.[22] Also, every Si_{2p} spectra exhibited (Figure S8: XPS analysis) a broad distribution centered around 102.5 eV, attributed to Si−O−C linkage, which supports the grafting of SCA.[23] Therefore, the observed increment of silicon content in tandem with the trade-off decrement of oxygen content (Table S1) can be regarded as a sign that the condensation reaction between silanol and hydroxyl groups on CF_{Ox} gave rise to two covalencies, Si−O−C and Si−C, on the SCA-grafted CF surfaces. Further, we obtained detailed evidence of grafting via C_{1s} high-resolution spectra. In the cases of $CF_{Ph\text{-}Az\text{-}S}$ and $CF_{An\text{-}Az\text{-}S}$ (Figure 3e,f), the broad peak centered around 291.1 eV, which is assigned to $\pi-\pi^*$ carbon satellites, appeared due to aromatic stacking of the benzyl rings from the grafted SCAs containing a phenyl unit.

To further study the origin of nitrogen species on the functionalized CF, the N_{1s} spectra of CF were obtained; this afforded the differentiation of the chemical nature of CF (Figure 4). For instance, the azide group can be inferred by the presence of the two distinct broad peaks centered at 400.4 and 404.3 eV.[24] On the other hand, in the N_{1s} spectra of $CF_{Ph\text{-}Az\text{-}S}$ and $CF_{An\text{-}Az\text{-}S}$, the peak at 404.3 eV disappeared and the peak at 400.4 eV shifted to higher binding energy around 401 eV, indicating, in this case, the formation of an unsaturated nitrogen species (−N═N−) originating from the triazole moieties.[25] On the contrary, $CF_{An\text{-}Az\text{-}S}$ exhibited a peak at a lower binding energy around 398.5 eV, which could be attributed to the primary amine from the aniline structure.[26]

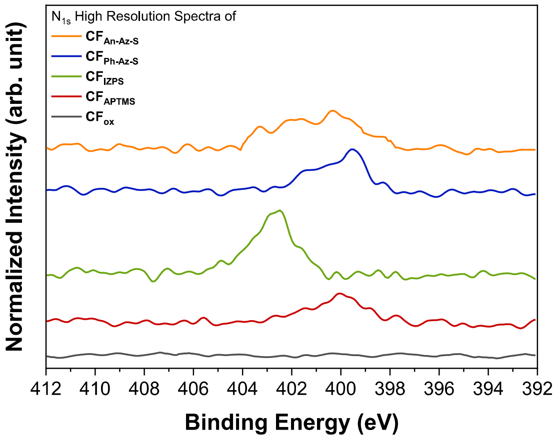

Figure 4. N_{1s} high-resolution spectra of carbon fibers with or without SCAs; CF_{Ox}, CF_{APTMS}, CF_{IZPS}, $CF_{Ph\text{-}Az\text{-}S}$, and $CF_{An\text{-}Az\text{-}S}$.

(Incidentally, no spectroscopic peaks associated with the copper metal residue were observed from the survey spectra of the functionalized CF with click SCA (Figure S7: XPS analysis—survey scan), which validates that the copper catalyst was removed entirely after the click reaction.)

2.2. Effects of Click SCA on Epoxy Curing Kinetics. In reports focused on the epoxy/dicyandiamide (DICY) system's cure mechanism, the general opinion supports a series of complex reactions from the straightforward epoxy-amine addition reaction to the chaotic propagation affording a three-dimensional cross-linked structure.[27] For this, the use of the temperature-resolved attenuated total reflection-Fourier transform infrared (ATR-FTIR) spectroscopy to track the resin's chemical changes during a sequential thermal program can provide a piece of corroborative evidence for deducing the cure mechanism. The IR spectra of epoxy/DICY and epoxy/DICY/An-Az-S systems were summarized and shifted along the ordinate for clarity (Figure 5). It should be noted that the used epoxy resin initially bears ether linkages attributed to the condensation reaction between the diglycidyl ether bisphenol A backbone and a glycidyl group in the silicon precursor by the manufacturer.

In the IR spectra of the epoxy/DICY system (Figure 5a,b), the characteristic bands corresponding to the sequential products of the epoxy cure reaction showed varied intensity as the system temperature increased. Two characteristic bands belonging to nitrile (−C≡N) in the DICY molecule at 2153 and 2207 cm^{-1} in reaction stage A were converted to the sharp band at 2150 and 2170 cm^{-1} after reaching stage E due to the formation of alkylated DICY.[28] With regards to changes in functional groups of the epoxy resin, the characteristic bands at 912 and 1111 cm^{-1} were worthy of attention, each associated with the epoxy group (−CH(O)CH−) and the ether group (−C−O−C−), respectively. As the temperature rises, the absorption band at 912 cm^{-1} progressively diminishes, and the sharp band at 1111 cm^{-1} becomes broadened. This might suggest the initial disintegration of the epoxide group via etherification with hydroxyl groups at the higher reaction stage from C to E.[29] The hydroxyl groups were formed by the epoxy ring−opening reaction signifying a shift in characteristic bands from 3420 and 3380 cm^{-1} (i.e., the amine group in DICY) to the broad band at 3400 cm^{-1} (i.e., hydroxyl groups in the cure intermediates).

Along with that, there are three additional weak to medium bands at 1734, 1650, and 1590−1550 cm^{-1}, with increased absorption intensities yielding information of possible reactions during the epoxy cure process. The absorption bands at 1734 and 1650 cm^{-1} were associated with the carbonyl group of the amide bond in 2-oxazolidone (formed by the hydrolysis at the imide bond) and the imino groups (formed by the intermolecular addition of hydroxyl to the DICY cyano functionality), respectively.[28] It seemed that the amide formation reaction continually occurred at the later reaction stage of C to E, which augments the complexity in the

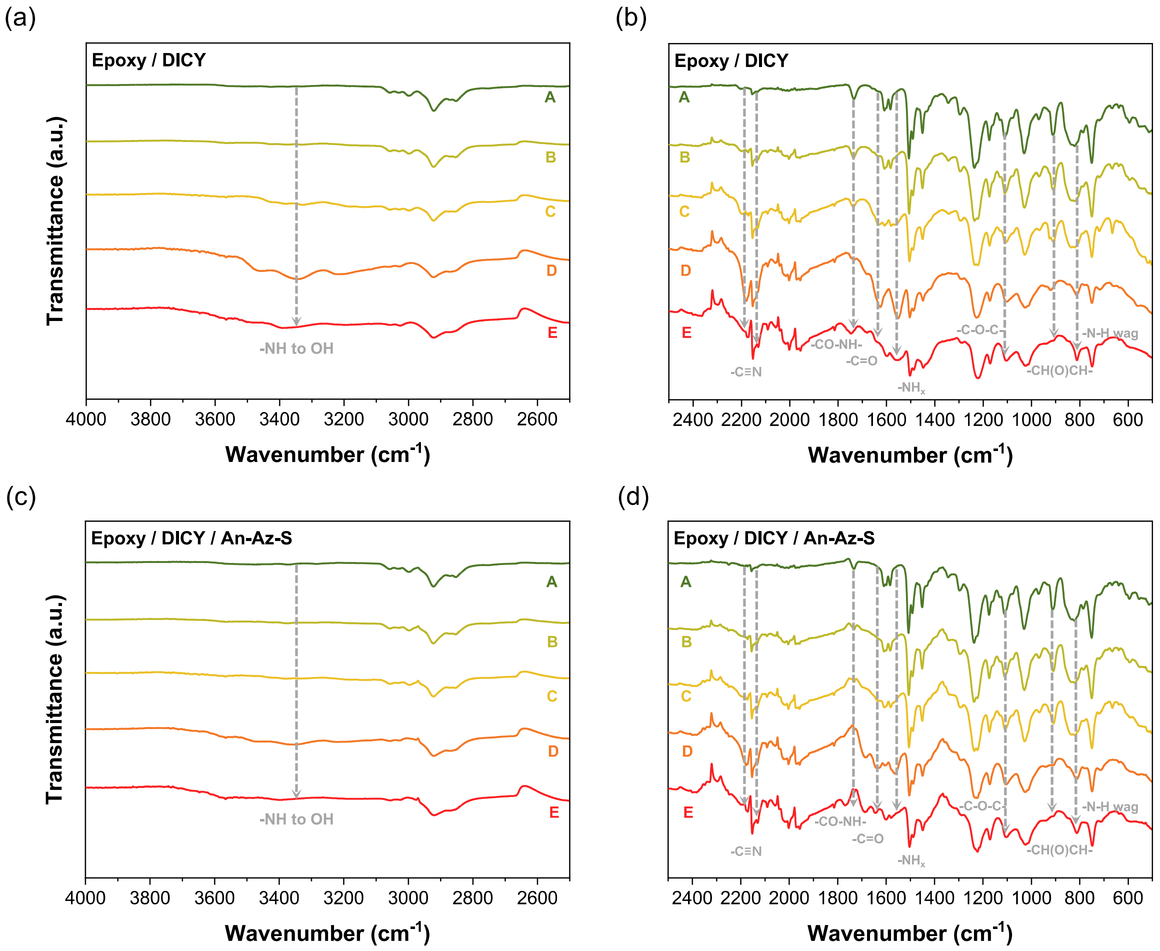

Figure 5. IR spectra of the epoxy/DICY system, (a) 4000−2500 and (b) 2500−500 cm^{-1}, and the epoxy/DICY/An-Az-S system, (c) 4000−2500− and (d) 2500−500 cm^{-1}, collected in different curing stages at (A) 50, (B) 100, (C) 150, (D) 200, and (E) 250 °C.

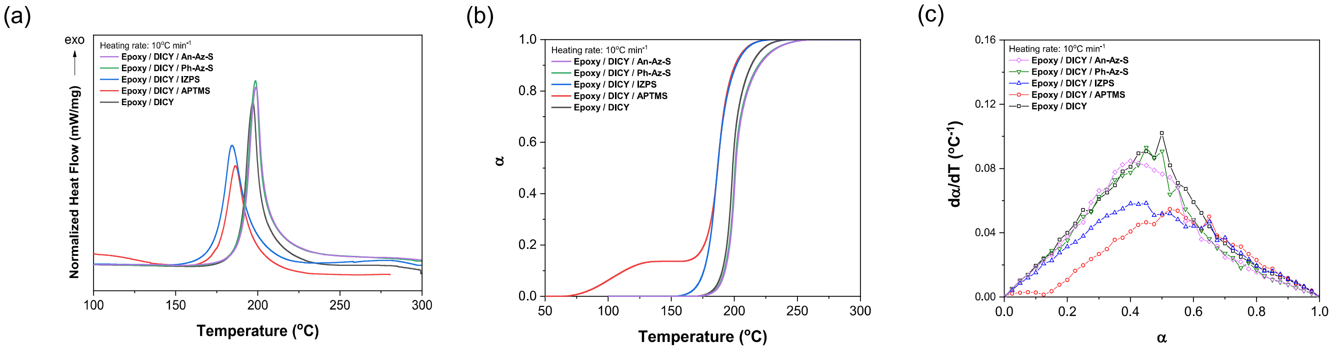

Figure 6. Plots from the DSC analyses on the epoxy/DICY and with or without SCA: (a) heat flow curve, (b) conversion, and (c) reaction rate obtained from the temperature sweep at the heating rate of 10 °C min^{-1}.

cross-linking reaction, accompanying the series of structural rearrangements of imine and amide intermediates[27] —the advent of a broad absorption band at 1590−1550 cm^{-1} corresponding to $-NH_x$ stretching supports this. In light of the changes in band absorptions, one can establish and assort the epoxy/DICY system's cure reaction into two sequential reactions; the epoxy-amine addition reaction throughout the cure process and the amide formation reaction at the higher reaction temperature.[30,31]

In the epoxy/DICY/An-Az-S system (Figure 5c,d), analogous characteristic bands appeared and shifted similar to the epoxy/DICY system during a thermal cure. Notice that the increase of the absorption bands corresponding to the amide formation reaction (1750, 1660, and 1560 cm^{-1})[29] was enhanced in the way of stage A to E. This could be ascribed to the contribution of a triazole moiety in the An-Az-S molecule to the amide formation reaction, yielding amides or $-NH_x$ groups. The triazole's nitrogens have the potential for reactivity that attacks the electron-deficient carbon in the epoxy, forming the epoxy-triazole adduct, suggestive of a tertiary amine activation reaction of an epoxide catalyzing epoxy ring-opening.[27] Another possible reaction is the epoxy homopolymerization initiated by nucleophilic addition of the DICY-protonated triazole. The intermolecular addition of a

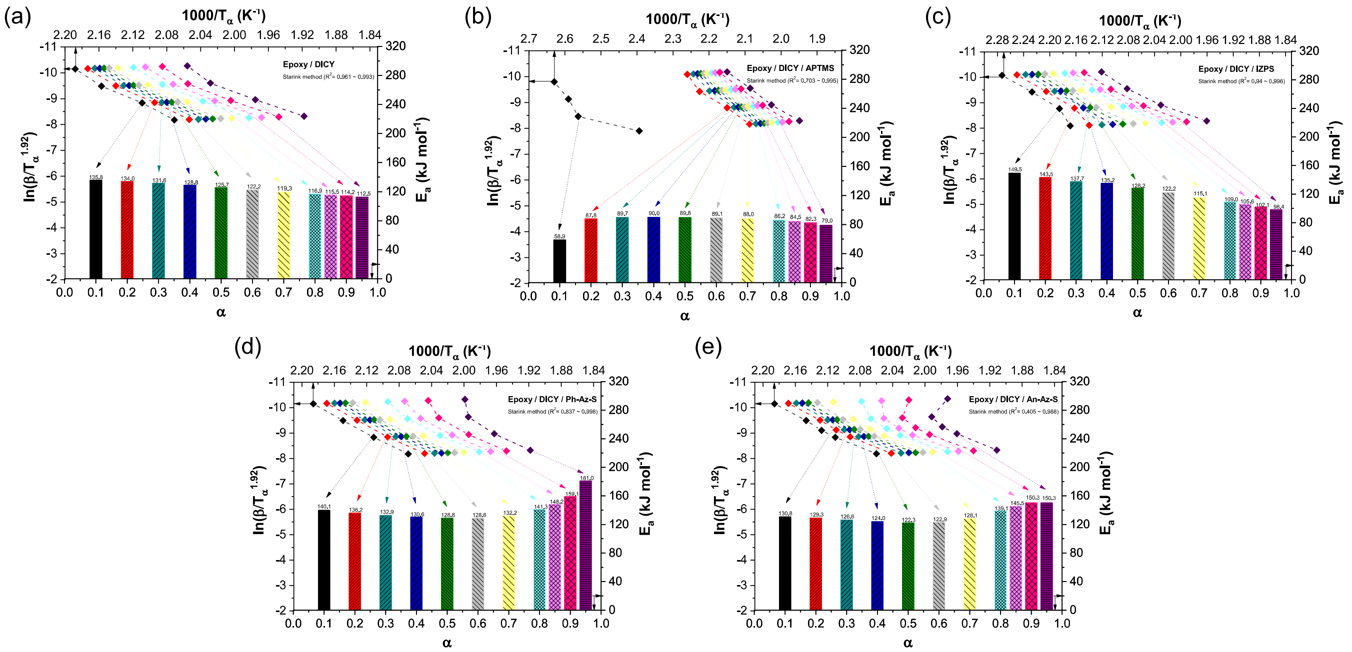

Figure 7. Starink plots and activation energy analyses for the (a) epoxy/DICY, (b) epoxy/DICY/APTMS, (c) epoxy/DICY/IZPS, (d) epoxy/DICY/Ph-Az-S, and (e) epoxy/DICY/An-Az-S.

tertiary amine to the hydroxyl group in the *N*-alkyl cyanoguanidine molecule can induce amide formation and epoxy homopolymerization. It could have been evidenced via the point when the absorption band for the triazole moiety up-shifted; however, the unavoidable CO_2 noise around 1900–2100 cm^{-1} when heating the FTIR–ATR plate screened the characteristic band of the triazole moiety and impeded the direct detection. The IR spectra for the systems including 3-aminopropyltrimethoxysilane (APTMS), triethoxy-3-(2-imidazolin-1-yl)propylsilane (IZPS), and Ph-Az-S are listed in the electronic Supporting Information (Figure S9: IR analyses for the epoxy/DICY/SCA systems).

We took a different approach, therefore, in an attempt to understand the role of each SCA in the epoxy cure reaction; the exothermic curve, the evolution of extent of conversion *α* with temperature, and the reaction rate d*α*/dt versus *α* at the heating rate of 10 °C min^{-1} were plotted (Figure 6a–c, respectively) by using differential scanning calorimetry (DSC) analysis (no thermal degradation occurred within the range of heating program, Figure S10). The precocious advents of an exothermal peak of the epoxy/DICY/APTMS and the epoxy/DICY/IZPS systems were attributed to the presence of a primary amine and 2-nitrogen atom having unpaired electrons exhibiting nucleophilic reactivity to form a 1:1 adduct (O^-) with an epoxy group, respectively. This enables the O-etherification reaction for the epoxy cure.[32] On the contrary, the thermograms of the epoxy/DICY system with click SCA exhibited different exothermic behavior, which involved a shift to a higher temperature range with increased heat flow, especially at a higher temperature as noted in the IR analyses. This latent reactivity of the click-derived molecules toward the later stage of epoxy cure becomes of particular interest and a focus of discussions hereafter.

To delve into the effects of the click SCA on each system's epoxy cure, we used the isoconversional method to interpret cure kinetics. Along with a non-isothermal cure program, the thermographs of weight-normalized heat flow as a function of temperature at different heating rates were obtained and are presented in Figure S11 and S12, while the corresponding analytical results are listed in Table S2. The amount of SCA included in the epoxy/DICY system was consistent in all runs with 6.5 mol % with respect to the DICY quantity revealing the highest Δ*H* (Table S3). All heat flow curves uniformly presented one exothermic peak irrespective of heating rates and types of SCA, indicating that the epoxy/DICY with SCA systems undergo one combined exothermic stage and no further cure reaction occurs over 290 °C. As the heating rate increased, expectedly, every exothermic peak shifted to the higher temperature range with an expanded full width at half the height of the exothermic peak, while the total cure reaction enthalpy (Δ*H*) was consistent with the experimental error limit (within 10% of the average value). That is, even when the heating rate ascended, the epoxy/DICY/SCA system experienced a similar main exothermic event expected from the epoxy cure process with comparable extents of the reaction.

A particularly notable event was that the runs with click SCA proceeded with a much more intense cure experience (Δ*H* ∼ 350–370 J g^{-1}) compared to those of the epoxy/DICY system or the epoxy/DICY/SCA without a triazole moiety (Δ*H* ∼ 277–315 J g^{-1}). This indicated that the click SCAs with a triazole moiety intervened in the epoxy/DICY cure reaction steps and triggered the additional exothermic events; hence, the heat of enthalpy ascended. The most striking difference caused by the ingress of latent-curable components was well-manifested in the cure kinetic study, especially the activation energies of the cure reaction (E_a) obtained from the systems with or without the click SCA. As mentioned earlier, the isoconversional kinetic analysis is not sensitive to the types of kinetic models used and thus can be particularly helpful in recapitulating the complex cure mechanism and predicting the kinetics of thermosetting polymers. As stated in previous reports,[28,31] the cure reactions in the epoxy/DICY system involve at least two separate but overlapping reactions, involving the nitrile group or primary amine yielding the

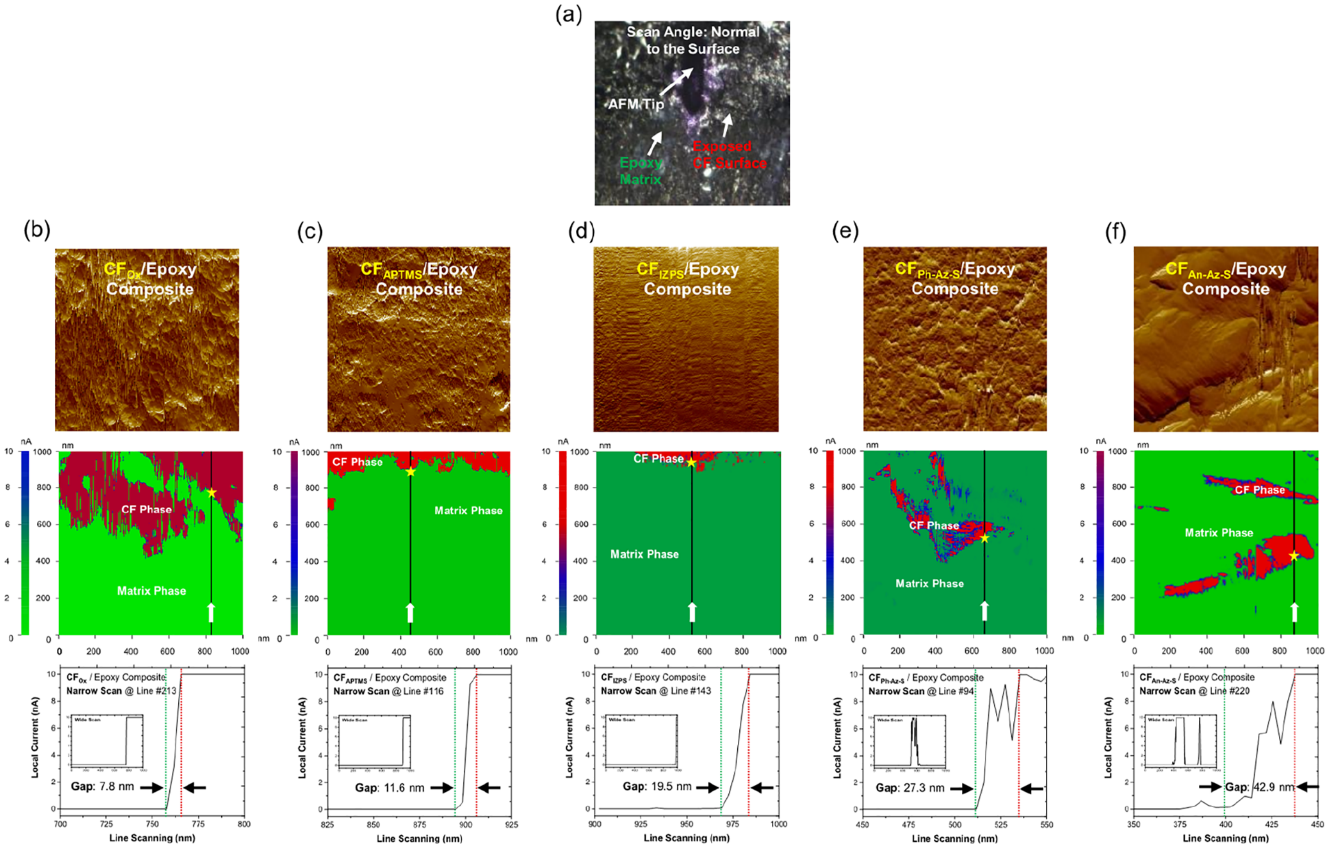

Figure 8. Conductive AFM analyses on the cross-section surface of the CFRP reinforced with the functionalized CF. (a) Screenshot at the microscopy observing window illustrating the conductive AFM tip vertically aligned to the surface. (b−f) Datasets for CFRP prepared with CF$_{Ox}$, CF$_{APTMS}$, CF$_{IZPS}$, CF$_{Ph\text{-}Az\text{-}S}$, and CF$_{An\text{-}Az\text{-}S}$; (top) error signal topography, (middle) local current mapping, and (bottom) sectional current analysis obtained from the black marked line with a white arrow at each local current map above.

oxazoline derivative or carbodiimides, and these intermediates further fused into complicated cross-linked products. Presumably, the E_a for the system consistently varies with the cure reaction progress, and the evolution of E_a can provide us with comparative information about cure behavior according to the resin mixture composition.

The E_a variation for the epoxy mixture systems with or without SCA as a function of the degree of conversion is displayed in Figure 7. Apparently, the E_a values immensely varied with respect to conversion, revealing the cure reactions of epoxy/DICY and epoxy/DICY with the SCA obeying multistep kinetics with varying thermal barriers. The highest initial E_a generally is attributed to the non-autocatalyzed reaction behavior at the beginning of a cure process.[33] For the epoxy/DICY system with no additives (Figure 7a), the E_a decreased steadily from 135.8 to 112.5 kJ mol^{-1} throughout the entire cure progress. At the early stage, the formation of a trimolecular transition state of amine-epoxy-hydroxyl must take precedence for epoxy chain extension, which constitutes the rate-determining step of the cure reaction. However, with the temperature rise, the reaction quickly shifted ($0 < \alpha < 0.2$) to an autocatalytic mode, given that the hydroxyl groups generated from the epoxy-amine addition reaction facilitate the epoxy ring−opening reaction. The enhanced molecular mobility and diffusion of the components also play a significant role in expediting reactive collisions between them.[29] On the other hand, albeit the hazy line of demarcation, the decline in E_a in the later stage ($\alpha > 0.6$) is assumed to have a basis different from the earlier one. Reportedly,[34] the transition of the regime from the kinetically controlled cure to the diffusion-controlled cure occurs as of the end of vitrification. On route to approaching an optimal state of cross-linking, the system enters the diffusion-controlled regime. The remaining small reactants start to diffuse within confined lattices, resulting in lower E_a, and the reaction reaches an end. Similarly, the evolutions of E_a for the epoxy/DICY/APTMS system and epoxy/DICY/IZPS (Figure 7b,c) also displayed an attenuating dependency on heat and conversion. The consistent decline in E_a at a later stage denotes that both APTMS and IZPS molecules have no additional contribution to cross-linking at higher conversion.

Once we introduced the click SCA into the resin mixture, the trend completely turned around. In the earlier stage ($0 < \alpha < 0.5$), the E_a for the epoxy/DICY/Ph-Az-S system (Figure 7d) slightly decreased from 140.1 to 128.6 kJ mol^{-1}, demonstrating a typical amine-epoxy addition cure behavior. Surprisingly, as α reached over 0.6, the sudden upturn of variation and progressive gain in E_a were observable in contrast to the former cases, which exhibited a continuous decline in E_a irrespective of the reaction progress. The epoxy/DICY/An-Az-S system also showed a similar trend when the E_a values were slightly lower than those from the Ph-Az-S based system because of the primary amine structure in the An-Az-S. A similar result of burgeoning E_a at the later stage of cure reaction of the epoxy/amine or the epoxy/DICY can also be found in previous reports, ascribing this to the homopolymerization of longer epoxy chains and the decreased molecular mobility after the vitrification of the system.[29,35] In this

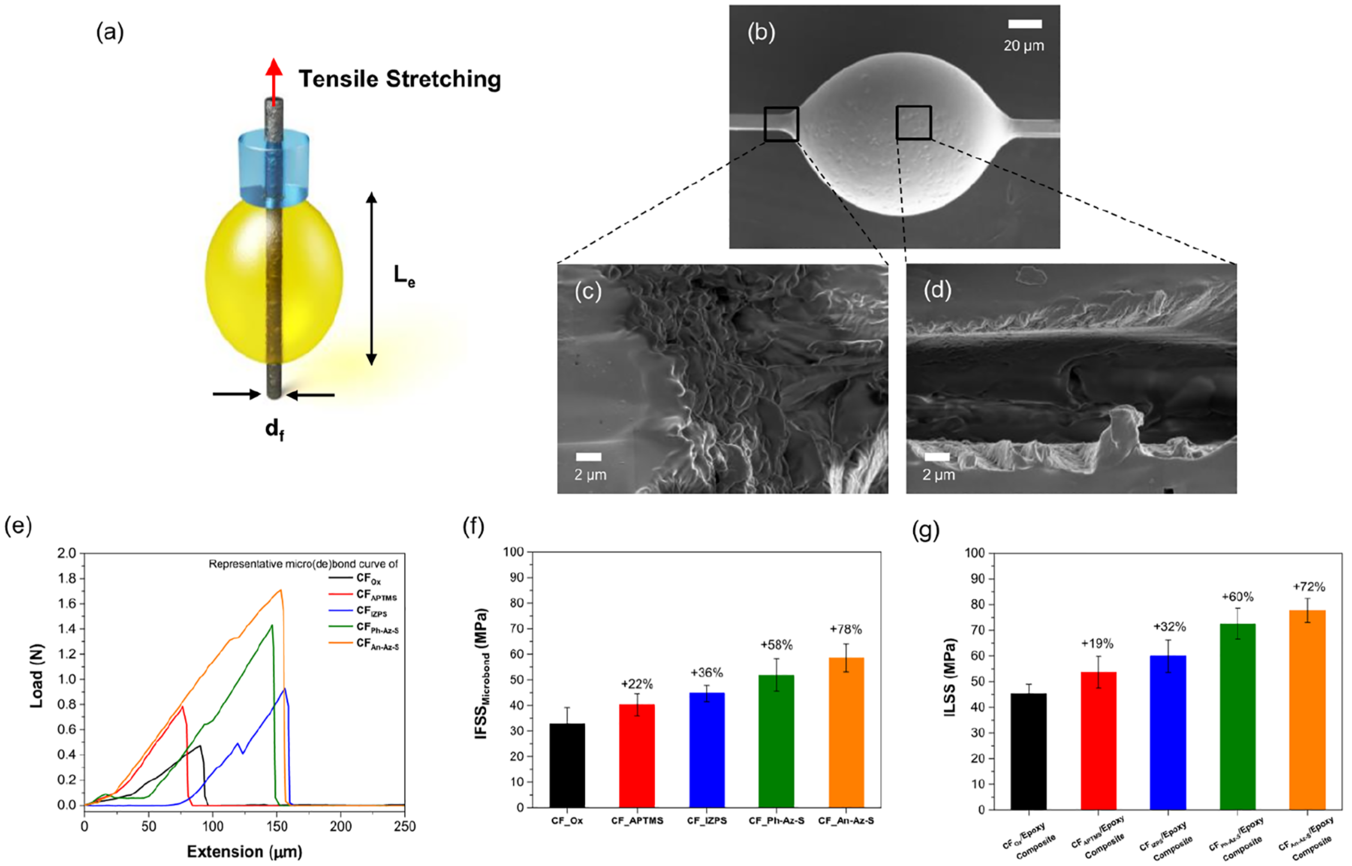

Figure 9. (a) Schematic design of micro(de)bonding test. d_f is the diameter of the fiber and L_e is the fiber's embedded length in an epoxy droplet. (b) Microdroplet sample observed by SEM before debonding. (c) Torn surface of the fiber and the (d) escaped epoxy droplet after debonding. (e) Typical microdroplet force−displacement curves recorded during tensile stretching, (f) resultant IFSS, and (g) ILSS obtained from CF/epoxy composites reinforced by the functionalized CF; CF_{Ox}, CF_{APTMS}, CF_{IZPS}, $CF_{Ph-Az-S}$, and $CF_{An-Az-S}$. (f−g) Data are presented as mean values ± s.d.

context, we assumed that both the Ph-Az-S and An-Az-S molecules, especially the triazole moiety, reacted as a cross-linking agent to generate junction points between the epoxy network chains, begetting a more close-packed cross-linking structure in response to the increased energy barrier required for the cross-linking reaction to occur rapidly as the reaction progressed till completion ($\alpha < 0.95$). We want to emphasize that the effect over the later cure progress ($\alpha > 0.6$) clearly shows the latency of Ph-Az-S and An-Az-S and their specified contribution to the epoxy cross-linking reactions. This result implies that incorporating the triazole SCA induces an enhanced cross-linking within the epoxy resin system as long as ample heat is provided into the resin mixture. For the validation of the hypothesis, several optical and mechanical evaluations on the CF/epoxy interface were conducted in the following sections.

2.3. Exploring the Interphase between the CF and Epoxy.

Conductive atomic force microscopy (AFM) was utilized to probe the local electrical properties of the interphase region between the CF and epoxy resin phases, where the former showed conductivity while the latter did not. The cured epoxy/CF specimen's topography was acquired from the cantilever tip's oscillating signal contacting the sample surface. At the same time, the bias voltage was applied between the tip and the sample surface via a conductive cantilever, and an electric current amplifier measured the induced tunneling current. When the AFM tip encountered the transverse face of the exposed CF (Figure 8a) while positioning the expanse of the epoxy matrix, the current signal was acquired and mapped ($1 \times 1\ \mu m^2 = 256 \times 256$ pixels^2).

For the current signal topographies of CF_{Ox}, CF_{APTMS}, CF_{IZPS}, $CF_{Ph-Az-S}$, and $CF_{An-Az-S}$, one can observe stark differences among the composites (Figure 8, middle). While all local current maps consisted of three regions—nonconductive (green, epoxy), moderate (blue, interphase), and conductive (red, CF)— each map obtained can be distinguished by its colorimetric distribution. The composite with CF_{Ox} showed a sharp contrast in current signals from 9 pA to 10 nA obtained from the matrix and fiber region (Figure 8b, bottom). The gap between the highest and lowest current only reaching a magnitude of 7.8 nm in length shows only minor interphase,[36] which denotes that the cure of epoxy resin does not necessarily signify the physicochemical linkage to the CF surface. The composites with CF_{APTMS} and CF_{IZPS} displayed an extended gap of current transition signal (Figure 8c,d, bottom), showing that the chemi/physisorbed silane layer on the CF surface is effective in forming the interphase. Plus, on account of the contributions of APTMS and IZPS molecules to the epoxy cure reaction as discussed in the DSC analyses, the chemical cross-linking between the grafted silane layers and the surrounding epoxy resulted in the current gap registering higher values (ca. 11.6, 19.5 nm, respectively) than that of the composite with CF_{Ox}. The cross-linking-derived interphase expansion is well demonstrated with the composites with the SCA-grafted CF (i.e., $CF_{Ph-Az-S}$ and $CF_{An-Az-S}$, Figure 8e,f). There are remarkable extensions of

https://doi.org/10.1021/acsomega.2c00045

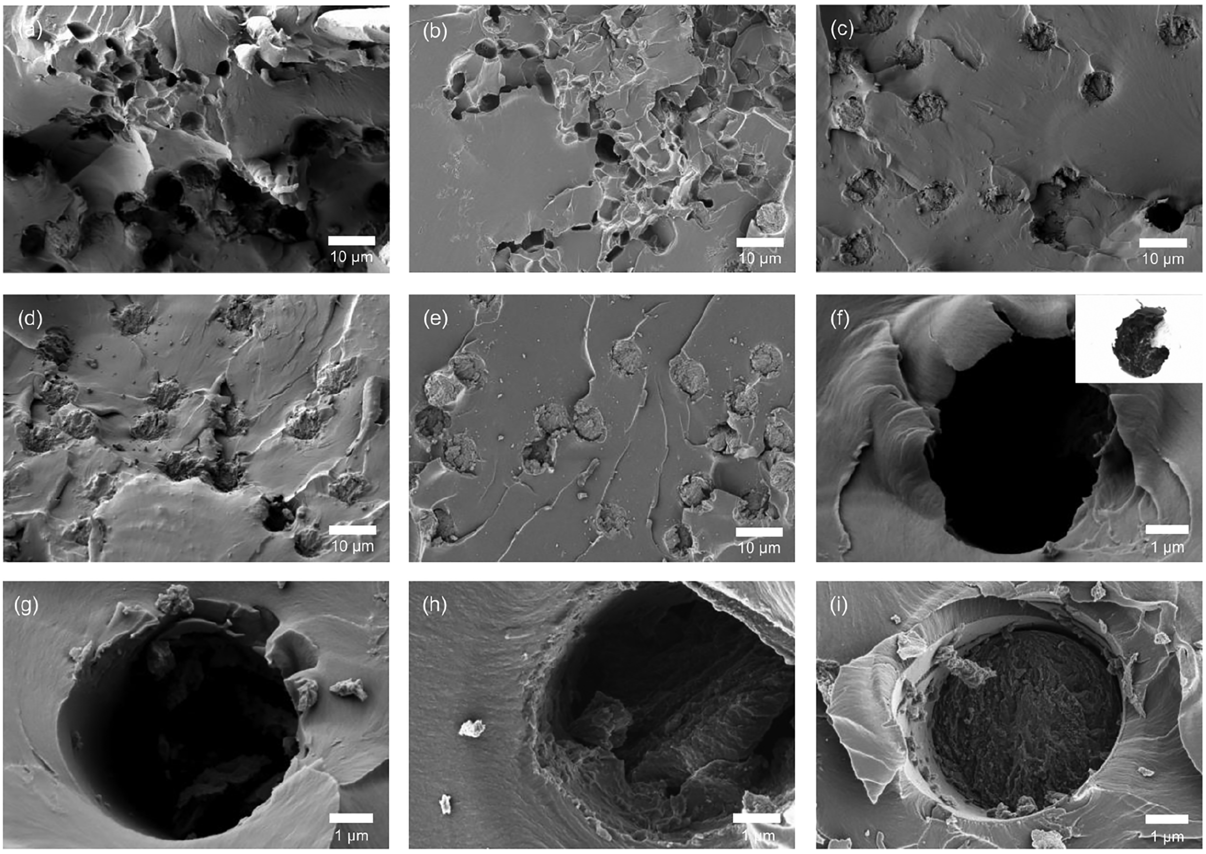

Figure 10. SEM micrographs of fractured surface morphologies obtained after the ILSS bending test for the composites reinforced with (a−e) CF_{Ox}, CF_{APTMS}, CF_{IZPS}, $CF_{Ph\text{-}Az\text{-}S}$, and $CF_{An\text{-}Az\text{-}S}$ at ×3000 magnification. The resulted void morphologies from the composites reinforced with (f,g) CF_{Ox} and CF_{APTMS} at × 15 000 magnification, (h) $CF_{Ph\text{-}Az\text{-}S}$ at ×20 000 magnification, and (i) $CF_{An\text{-}Az\text{-}S}$ at ×15 000 magnification.

moderate current transition region reaching about max. 42.9 nm, recording an approximately 6-fold rise (compared to that of the composite with CF_{Ox}). From the line analyses on current signals (Figure 8e,f, bottom), it can be seen that the gradient of the current signal is less steep, indicating that the current transition region at the interphase is expanded. From the molecular structural distinction between CF_{APTMS} and $CF_{An\text{-}Az\text{-}S}$, by intuition, we can relate the triazoles to the interphase expansion where the covalency between the multisorbed triazole moieties on the CF and epoxy chains add intricateness during the epoxy cross-linking reaction. This was already inferred in the DSC analysis that the increased ΔH and E_a for the epoxy/DICY with the triazole SCAs suggested an enhancement in cross-linking. It appeared that the newly formed covalent bonds with the triazole-modified CF and epoxy matrix gave rise to the formation of interphase, which effectively enhances the interfacial adhesion properties and acts as a stress-transfer region from which the immense load on the composite would be exerted. This assumption inspired us to test the mechanical properties of the composites reinforced by the SCA-grafted CF.

2.4. IFSS of Single-Fiber Composite, ILSS, and Fractography of CFRP.

To assess the impact of enhanced cross-linking between the epoxy and CF surface on the interfacial adhesion strength, a micro-debonding test for IFSS of the single fiber composite and a three-point short beam test for interlaminar shear strength (ILSS) of CFRP were performed. For the micro-debonding test, a cured microdroplet (ca. 90 μm in diameter) epoxy/DICY mixture was set beneath a steel tube with an inside diameter of 50 μm to avoid microdroplet tagging when the fiber is being pulled by a tensile grip (Figure 9a). The single fiber composite reinforced by CF_{Ox} yielded the lowest IFSS of 32.9 MPa. It is noteworthy that the CF_{Ox} was selected as the control sample since all functionalized fibers originated from this. Hence, the cause of enhancement of IFSS values was only accounted for the effect of the surface functionalization. To this end, the IFSS gains of single-fiber composites with the functionalized CF prove that silane grafting effectively enhances interfacial mechanical properties, as stated in the previous study.[37] The distinguishable result is obtained from the single-fiber composite reinforced by $CF_{An\text{-}Az\text{-}S}$, recording a considerable enhancement in the IFSS to 58.7 MPa to 78% increment in the value of the CF_{Ox} composite and even surpassing that of the CF_{APTMS} composite by a wide margin (ca. +46%). After debonding, the skin of the fiber embedded before was completely stripped down, and marks of interfacial failure were left on the $CF_{An\text{-}Az\text{-}S}$ surface (Figure 9c). Similarly, the lacerated wound on the escaped epoxy droplet showed waves and patchy dents at the interface on account of the strong shear effect[38] responsible for the IFSS gains (Figure 9d).

The reinforcement of pull-out adhesion strength can be explained in a couple of adhesion mechanisms, covering the newly extended interphase between epoxy and CF. (1) From the perspective of surface chemistry, the grafted SCA can generate newly formed surfaces with a greater chemical affinity toward the epoxy and the hardener molecules. Hence, the wetting and adsorption of the epoxy matrix against the CF

Figure 11. Schematic conceptual design of the interfacial cross-linking between epoxy resin and the triazole-tethered CF (left) before and (right) after the latent cure reaction.

surface were enhanced.[18] This consideration was supported by measuring the changes in the CF's surface chemistry followed by silane deposition (Figure S9). The increased hydrophobicity of the CF's surface would allow the epoxy resin to be wet and interact better with the surface. (2) In view of the physical interlocking mechanism, the grafted molecules might act as dangling "beanstalk,"[9] defying shear force at the bicomponent interface. Similar degrees of enhancements on IFSS (+70 ~ 130%) or ILSS (+40 ~ 70%) were reported via grafting polymers[39,40] or high-molecular sizing agents[41] recently, while this paper used low-molecular curatives which can be further utilized. The mechanical interlocking at the CF surface can be superimposed by the overlapped interface from multiadsorbed silane layers. However, it does not suffice to explain the higher IFSS of composites reinforced by the triazole SCA when the quantity of deposited SCA and the wetting property of CF_{APTMS} and $CF_{An\text{-}Az\text{-}S}$ showed comparable results (Figure S9); (CF_{APTMS}) 65° of WCA and 3.7 mequiv g_{fiber}^{-1} of $W_{grafted}$ and ($CF_{An\text{-}Az\text{-}S}$) 75° of WCA and 4.0 mequiv g_{fiber}^{-1} of $W_{grafted}$, both at the silane doses of 20 mmol/g_{CF}. Such as the case is, we propose an alternative explanation. As discussed in the IR and DSC analyses, the SCA with triazole moieties has the ability to react with epoxide groups to form a covalently cross-linked complex network within the resin/fiber interphase. In addition to this, in the case of the $CF_{An\text{-}Az\text{-}S}$ composite, the primary amine attached to the aniline structure could also contribute to the amide formation reaction. Here, the highest ILSS gain was obtained. It appears the surface-tethered reactive molecules provide ready-to-cure sites and the cure reaction invokes expanded cross-linking between the fiber and the matrix, which consequently enhances the pull-out adhesion strength. The ILSS of CFRP showed a similar tendency of enhancement (Figure 9g). While the composite reinforced by CF_{Ox} recorded only 45 MPa, the composite with CF_{APTMS}, CF_{IZPS}, $CF_{Ph\text{-}Az\text{-}S}$, and $CF_{An\text{-}Az\text{-}S}$ recorded 54, 60, 72, and 78 MPa, respectively, in a stepwise manner.

After the three-point bending test, we collected the fractured specimens and observed the cross-sectional SEM morphologies (Figure 10). One can see that there are signs of severe fiber pull-out and resultant voids throughout the epoxy matrix in the composites reinforced by CF_{Ox}, and CF_{APTMS} (Figure 10a,b). As a corollary of weak adhesion, the interphase between the fiber and matrix could not efficiently deliver the external shear load and completely collapsed, leaving a cleanly fractured surface at voids (Figure 10f,g). (The legend on Figure 10f shows the inside of the void, manifesting no sign of fiber residue left therein.) Contrary to this, the CFRP prepared with the IZPS, Ph-Az-S, and An-Az-S presented better interfacial adhesion with the structural feature with fewer voids from fiber-pulling (Figure 10c–e) when fibers remained steady within the matrix, which is the reason for ILSS gains. Upon closer examination, the $CF_{Ph\text{-}Az\text{-}S}$/epoxy and $CF_{An\text{-}Az\text{-}S}$/epoxy composite's fractured surface appeared to be continuous (Figure 10h,i) so that each modified CF and the matrix were inextricably intertwined by chemical cross-linking during the epoxy curing process as expected in the former sections. Since the continuous interphase could serve as a transition layer, when flexural stress is applied, the stress should effectively be dissipated through the medium, thereby circumventing the adhesive failure at the CF surface. In consideration, it may be natural for the ILSS of the CFRP with the triazole-functionalized fibers (77.8 MPa) to outrun the ILSSs of the CF_{Ox}/epoxy (45.3 MPa) and even the CF_{APTMS}/epoxy composite (53.7 MPa), which suffer from an insufficient matrix/fiber interface as revealed in the conductive AFM characterization.

3. CONCLUSIONS

To improve both cure and interfacial properties, we have fabricated the click-derived SCA and successfully grafted them on CF surfaces as confirmed by XPS and contact angle analysis. The effects of click SCA on the cure reaction for the epoxy/DICY system were highlighted and were comparatively characterized by the DSC analysis. It was revealed that approximately 20% increased degree of total reaction enthalpy was obtained in the curing reaction of the epoxy/DICY with the click SCA system. Moreover, the activation energy of the epoxy/DICY/Ph-Az-S system drastically overturned its dependency on conversion on the verge of the cross-linking point and hit a maximum of 180 kJ mol^{-1} at the final stage of the curing process ($\alpha \sim 0.95$). This is clearly distinguished from those obtained from epoxy/DICY without the triazole SCA systems. The role of a triazole moiety as a latent cure agent was also evidenced by the IR result augmented by the intensity of absorption bands corresponding to the amide formation reaction during the cure reaction of the epoxy/DICY/An-Az-S system. This potentially bestowed the heat-activated cross-link ability to the surface, facilitating the formation of covalent bridges connecting them to the epoxy matrix (Figure 11). Tracking of local currents on the $CF_{An-Az-S}$/epoxy composite by conductive AFM presented explicit evidence of the expansion of the interphase between the epoxy matrix and CF as a result of enhanced cross-linking by the click-derived end groups on the CF surface in contrast to the case of CF_{APTMS}/epoxy with no curable surface functionalities. The ILSS values were significantly increased (+72% in $CF_{An-Az-S}$/epoxy composite compared to the CF_{Ox}/epoxy composite) for the click-functionalized CF within which the extended interphase enhances its stress transferability and consequently mitigates catastrophic pull-out failure.

This paper shows several facets in the methodology of surface engineering and aspects of validating methods effective in improving interfacial adhesion for structurally related SCA. The "graft-to" methods for the preparation SCA prior to application on the oxidized CF surface in ethanol/water solution seem beneficial both to manufacturing and environmental aspects. Second, the preinstallation of a reactive platform on a CF surface grants a latent cross-linkability to it, which is crucial for attaining process-tailored cure properties and desired extents of conversion without a need of changing a resin recipe. This gratifies the required interfacial adhesion strength for final CFRP products irrespective of prepreg processing methods used. Finally, by virtue of numerous alkyne candidates (not the case in azides), the reactivity of the grafted surface toward epoxy cure reaction could be further modulated by engineers based on the desired application.

4. EXPERIMENTAL SECTION

4.1. Materials. The carbon fibers used in the experiments were PAN-based type. They consist of unsized and untwisted yarn, with 12 000 filaments per tow, and were kindly supplied by Toray Advanced Materials Korea Inc. The matrix resin mixture in the study comprises a silane-modified epoxy resin, KSR 177 (Kukdo Chemical Co., Ltd., Republic of Korea). A dicyandiamide type curing agent, Dyhard 100S (AlzChem Group AG., Germany), with the mix ratio of the curing agent to the epoxy resin was equivalent weight, 9.2 to 100 g. All chemicals, reagents, and solvents were purchased from Sigma-Aldrich, Inc., except 3-ethynylaniline (EA) purchased from Tokyo Chemical Industry Co., Ltd., and used as received.

4.2. Preparation of CuAAC Click SCA. Unless otherwise stated, all reactions were carried out in the air and using a liquid medium without degassing. ^{1}H NMR spectra were recorded on a 400 MHz spectrometer (JeolJNM-LA400 with LFG, Jeol, Japan) at room temperature. Chemical shifts (δ) are reported in ppm with respect to tetramethylsilane as an internal standard. IR spectra were measured by FTIR spectroscopy (Nicolet iS20, ThermoFisher Scientific, USA) equipped with a PIKE GladiATR ATR-accessory. The spectra were collected with a spectral resolution of 4 cm^{-1} in the range of 450−4000 cm^{-1}.

The representative procedure is as follows: Step 1, Formation of an azide-terminated silane: (Chloromethyl)-trimethoxysilane (10 mmol, 1.707 g) and sodium azide powder (13 mmol, 0.845 g) was bottled in 20 mL acetonitrile. The mixture was magnetically stirred at 500 rpm, 70 °C for 48 h to ensure the nucleophilic substitution reaction was completed. After the reaction mixture was separated using a centrifuge with 7000 rpm, the clear supernatant was only used in the following step. The FTIR spectrum of the mixture product was measured, and the characteristic IR adsorption band of azide groups around 2100 cm^{-1} was observed (Figure S1). Step 2, CuAAC click reaction: In a 20 mL vial fitted with a screw cap were loaded the above reaction mixture (1 equiv), alkyne (1 equiv. for each PA, and EA), and bromotris(triphenylphosphine)copper(I) (5 mol %). After completing the reaction over 3 h at room temperature, citric acid was added to reduce the copper catalyst, and the final product was obtained from the centrifuge isolation (Figure S2−S4).

4.3. "Grafting-to" Surface Functionalization on Carbon Fibers. Before the oxidation procedure, the filaments were washed with acetone to ensure all contaminants were eliminated. In the oxidation process, the dried CF bundles with a width of 5 mm were placed on the open stage of an atmospheric pressure plasma unit (PLAMI Auto-100, APP Co., Ltd., Republic of Korea). An RF power supply and AC with 200 W and 220 V, respectively, were applied. The dry airflow rate was set at 20 mL min^{-1} with Ar carrier gas (5 L min^{-1}). The bundles traveled back and forth from the plasma releasing line (100 W output), positioned 10 mm above the stage, exposing each side over 20 cycles with an exposure time of 10 s. This process fully oxidized the CF surface to saturation levels. A 5 cm length of the oxidized CF tow (approximately 41 mg) was instantly placed on a 50 mL borosilicate glass vial containing ethanol: water (9:1, v/v; pH of 5) medium (adjusted with hydrochloric acid). Each SCA, including APTMS, IZPS, 4-phenyl-1-((trimethoxysilyl)methyl)-1*H*-[1,2,3]triazol (Ph-Az-S), and 3-(1-((trimethoxysilyl)methyl)-1*H*-[1,2,3]triazole-4-yl)aniline (An-Az-S) of concentration 20 mmol/g_{fiber} were added and allowed to react under agitation of 150 rpm for an hour. The solvent was decanted, and the CF was gently swiped by acetone-soaked paper to eliminate the physisorbed silane layers on the surface. The surface-functionalized fibers were stored under reduced pressure until further use.

The detailed information on characterizations of the fibers' surface/interface and the resulting composites' mechanical properties is included in the electrical Supporting Information.

■ ASSOCIATED CONTENT

Supporting Information

The Supporting Information is available free of charge at https://pubs.acs.org/doi/10.1021/acsomega.2c00045.

Detailed characterization methods; IR and ^{1}H NMR spectra for the synthesized SCAs; and surface (contact angle, XPS) and thermo (thermogravimetric analysis, DSC) analyses on the SCA included systems (PDF)

■ AUTHOR INFORMATION

Corresponding Author

Hyun-Joong Kim − *Department of Agriculture, Forestry and Bioresources and Research Institute of Agriculture and Life Sciences, Seoul National University, Seoul 08826, Republic of Korea;* orcid.org/0000-0002-3897-7939; Phone: 2 880-4794; Email: hjokim@snu.ac.kr

Authors

Jae-Ho Shin − *Department of Agriculture, Forestry and Bioresources, Seoul National University, Seoul 08826, Republic of Korea;* orcid.org/0000-0001-5551-7734

Gi-Yeon Han − *Department of Agriculture, Forestry and Bioresources, Seoul National University, Seoul 08826, Republic of Korea;* orcid.org/0000-0002-3344-8536

Complete contact information is available at:
https://pubs.acs.org/10.1021/acsomega.2c00045

Author Contributions

J.-H.S.: conceptualization, investigation, methodology, visualization, and writing—original draft. G.-Y.H.: methodology and investigation. H.-J.K.: project administration, writing—review and editing, funding acquisition, and resources.

Notes

The authors declare no competing financial interest.

■ ACKNOWLEDGMENTS

This work was supported by the Ministry of Trade, Industry and Energy (MOTIE), Republic of Korea (grant number 10076899, Development of adhesive bonding technique for joining CFRP and other materials used for lightweight transportation equipment). We deeply thank Dr. Sonkaria Sanjiv for proofreading.

■ REFERENCES

(1) Gielen, D.; Newman, J.; Patel, M. K. Reducing Industrial Energy Use and CO2 Emissions: The Role of Materials Science. *MRS Bull.* **2008**, *33*, 471−477.

(2) (a) Mallick, P. K. *FiberRreinforced Composites: Material, Manufacturing and Design*; CRC Press, 2008. DOI: 10.1201/9781420005981. (b) Soutis, C. Fibre reinforced composites in aircraft construction. *Prog. Aeronaut. Sci.* **2005**, *41*, 143−151.

(3) Hernandez, D. A.; Soufen, C. A.; Orlandi, M. O. Carbon Fiber Reinforced Polymer and Epoxy Adhesive Tensile Test Failure Analysis Using Scanning Electron Microscopy. *Mater. Res.* **2017**, *20*, 951−961.

(4) Cartié, D. D. R.; Troulis, M.; Partridge, I. K. Delamination of Z-pinned carbon fibre reinforced laminates. *Compos. Sci. Technol.* **2006**, *66*, 855−861.

(5) (a) Jones, C. The chemistry of carbon fibre surfaces and its effect on interfacial phenomena in fibre/epoxy composites. *Compos. Sci. Technol.* **1991**, *42*, 275−298. (b) Pukánszky, B. Interfaces and interphases in multicomponent materials: past, present, future. *Eur. Polym. J.* **2005**, *41*, 645−662.

(6) Nicosia, C.; Huskens, J. Reactive self-assembled monolayers: from surface functionalization to gradient formation. *Mater. Horiz.* **2014**, *1*, 32−45.

(7) (a) Chen, J.; Lin, N.; Huang, J.; Dufresne, A. Highly alkynyl-functionalization of cellulose nanocrystals and advanced nanocomposites thereof via click chemistry. *Polym. Chem.* **2015**, *6*, 4385−4395. (b) Watson, M. A.; Lyskawa, J.; Zobrist, C.; Fournier, D.; Jimenez, M.; Traisnel, M.; Gengembre, L.; Woisel, P. A "clickable" titanium surface platform. *Langmuir* **2010**, *26*, 15920−15924.

(8) (a) Fang, M.; Zhang, Z.; Li, J.; Zhang, H.; Lu, H.; Yang, Y. Constructing hierarchically structured interphases for strong and tough epoxy nanocomposites by amine-rich graphene surfaces. *J. Mater. Chem.* **2010**, *20*(). DOI: 10.1039/c0jm01620a. (b) Peng, Q.; He, X.; Li, Y.; Wang, C.; Wang, R.; Hu, P.; Yan, Y.; Sritharan, T. Chemically and uniformly grafting carbon nanotubes onto carbon fibers by poly(amidoamine) for enhancing interfacial strength in carbon fiber composites. *J. Mater. Chem.* **2012**, *22*, 5928−5931. (c) Varshney, V.; Roy, A. K.; Michalak, T. J.; Lee, J.; Farmer, B. L. Effect of Curing and Functionalization on the Interface Thermal Conductance in Carbon Nanotube-Epoxy Composites. *JOM* **2012**, *65*, 140−146. (d) Holmes, G. A.; Feresenbet, E.; Raghavan, D. Using self-assembled monolayer technology to probe the mechanical response of the fiber interphase-matrix interphase interface. *Compos. Interfaces* **2012**, *10*, 515−546. (e) Xu, Z.; Zhang, J.; Shan, M.; Li, Y.; Li, B.; Niu, J.; Zhou, B.; Qian, X. Organosilane-functionalized graphene oxide for enhanced antifouling and mechanical properties of polyvinylidene fluoride ultrafiltration membranes. *J. Membr. Sci.* **2014**, *458*, 1−13. (f) Gemeay, A. H.; El-Halwagy, M. E.; El-Sharkawy, R. G.; Zaki, A. B. Chelation mode impact of copper(II)-aminosilane complexes immobilized onto graphene oxide as an oxidative catalyst. *J. Environ. Chem. Eng.* **2017**, *5*, 2761−2772. (g) Petersen, H. N.; F. Minty, R.; Thomason, J. L.; Yang, L.; Kusano, Y.; Brøndsted, P.; Almdal, K. The amine:epoxide ratio at the interface of a glass fibre/epoxy matrix system and its influence on the interfacial shear strength. *Compos. Interfaces* **2018**, *26*, 493−505. (h) Zhang, W.; Deng, X.; Sui, G.; Yang, X. Improving interfacial and mechanical properties of carbon nanotube-sized carbon fiber/epoxy composites. *Carbon* **2019**, *145*, 629−639.

(9) Demir, B.; Henderson, L. C.; Walsh, T. R. Design Rules for Enhanced Interfacial Shear Response in Functionalized Carbon Fiber Epoxy Composites. *ACS Appl. Mater. Interfaces* **2017**, *9*, 11846−11857.

(10) Chen, S.; Chen, L.; Wang, Y.; Wang, C.; Miao, M.; Zhang, D. Load transfer of thiol-ended hyperbranched polymers to improve simultaneously strength and longation of CNTs/epoxy nanocomposites. *Eur. Polym. J.* **2019**, *120*, 109254.

(11) (a) He, J.; Huang, Y.; Liu, L.; Cao, H. Controlled interface between carbon fiber and epoxy by molecular self-assembly method. *Mater. Chem. Phys.* **2006**, *99*, 388−393. (b) Feresenbet, E.; Raghavan, D.; Holmes, G. A. The role of the terminal functional group of self-assembled monolayers on fiber matrix adhesion. *J. Appl. Polym. Sci.* **2007**, *106*, 462−469. (c) Patil, V.; Dennis, R. V.; Rout, T. K.; Banerjee, S.; Yadav, G. D. Graphene oxide and functionalized multi walled carbon nanotubes as epoxy curing agents: a novel synthetic approach to nanocomposites containing active nanostructured fillers. *RSC Adv.* **2014**, *4*, 49264−49272. (d) Lee, S.; Suh, D.; Kim, W.; Xu, C.; Kim, T.; Song, C.; Yoo, C.; Kim, Y.; Kim, J.; Baik, S. Carbon nanotube covalent bonding mediates extraordinary electron and phonon transports in soft epoxy matrix interface materials. *Carbon* **2020**, *157*, 12−21.

(12) (a) Sekhavat Pour, Z.; Ghaemy, M. Polymer grafted graphene oxide: For improved dispersion in epoxy resin and enhancement of mechanical properties of nanocomposite. *Compos. Sci. Technol.* **2016**, *136*, 145−157. (b) Zhan, Y.; Wang, Y.; Wang, M.; Ding, X.; Wang, X. Improving the Curing and Mechanical Properties of Short Carbon Fibers/Epoxy Composites by Grafting Nano ZIF-8 on Fibers. *Adv. Mater. Interfaces* **2019**, *7*, 1901490.

(13) Zhao, X.; Huang, Z.; Song, P.; Chen, H.; Yang, H.; Zhang, Y. Effect of isophorone diamine on curing kinetics and mechanical properties of 2-ethyl-4-methylimidazole/epoxy resin crosslinked network. *Thermochim. Acta* **2019**, *680*, 178380.

(14) Lal, S.; Díez-González, S. [CuBr(PPh3)3] for Azide−Alkyne Cycloaddition Reactions under Strict Click Conditions. *J. Org. Chem.* **2011**, *76*, 2367−2373.

(15) Servinis, L.; Beggs, K. M.; Gengenbach, T. R.; Doeven, E. H.; Francis, P. S.; Fox, B. L.; Pringle, J. M.; Pozo-Gonzalo, C.; Walsh, T. R.; Henderson, L. C. Tailoring the fibre-to-matrix interface using click chemistry on carbon fibre surfaces. *J. Mater. Chem. A* **2017**, *5*, 11204−11213.

(16) Randall, J. D.; Eyckens, D. J.; Servinis, L.; Stojcevski, F.; O'Dell, L. A.; Gengenbach, T. R.; Demir, B.; Walsh, T. R.; Henderson, L. C. Designing carbon fiber composite interfaces using a 'graft-to' approach: Surface grafting density versus interphase penetration. *Carbon* **2019**, *146*, 88−96.

(17) (a) Ostaci, R.-V.; Damiron, D.; Capponi, S.; Vignaud, G.; Léger, L.; Grohens, Y.; Drockenmuller, E. Polymer Brushes Grafted to "Passivated" Silicon Substrates Using Click Chemistry. *Langmuir* **2008**, *24*, 2732−2739. (b) Fehr, J. M.; McKenas, C. G.; Liu, B.; Lockett, M. R. Azide-alkyne click reactions to prepare chemically modified amorphous carbon electrodes. *Appl. Surf. Sci.* **2019**, *480*, 1109−1115.

(18) Arnold, C. L.; Eyckens, D. J.; Servinis, L.; Nave, M. D.; Yin, H.; Marceau, R. K. W.; Pinson, J.; Demir, B.; Walsh, T. R.; Henderson, L. C. Simultaneously increasing the hydrophobicity and interfacial adhesion of carbon fibres: a simple pathway to install passive functionality into composites. *J. Mater. Chem. A* **2019**, *7*, 13483−13494.

(19) (a) Gardner, S. D.; Singamsetty, C. S. K.; Booth, G. L.; He, G.-R.; Pittman, C. U. Surface characterization of carbon fibers using angle-resolved XPS and ISS. *Carbon* **1995**, *33*, 587−595. (b) Hinterreiter, A. P.; Duchoslav, J.; Kehrer, M.; Truglas, T.; Lumetzberger, A.; Unterweger, C.; Fürst, C.; Stifter, D. Determination of the surface chemistry of ozone-treated carbon fibers by highly consistent evaluation of X-ray photoelectron spectra. *Carbon* **2019**, *146*, 97−105.

(20) Takahagi, T.; Shimada, I.; Fukuhara, M.; Morita, K.; Ishitani, A. XPS studies on the chemical structure of the stabilized polyacrylonitrile fiber in the carbon fiber production process. *J. Polym. Sci., Part A: Polym. Chem.* **1986**, *24*, 3101−3107.

(21) Lin, J.; Sun, C.; Min, J.; Wan, H.; Wang, S. Effect of atmospheric pressure plasma treatment on surface physicochemical properties of carbon fiber reinforced polymer and its interfacial bonding strength with adhesive. *Composites, Part B* **2020**, *199*, 108237.

(22) (a) Khung, Y. L.; Ngalim, S. H.; Scaccabarozzi, A.; Narducci, D. Formation of stable Si-O-C submonolayers on hydrogen-terminated silicon(111) under low-temperature conditions. *Beilstein J. Nanotechnol.* **2015**, *6*, 19−26. (b) Vashisth, A.; Khatri, S.; Hahn, S. H.; Zhang, W.; van Duin, A. C. T.; Naraghi, M. Mechanical size effects of amorphous polymer-derived ceramics at the nanoscale: experiments and ReaxFF simulations. *Nanoscale* **2019**, *11*, 7447−7456.

(23) Jiang, L.; Cheung, R.; Brown, R.; Mount, A. Inductively coupled plasma etching of SiC in SF6/O2 and etch-induced surface chemical bonding modifications. *J. Appl. Phys.* **2003**, *93*, 1376−1383.

(24) (a) Wollman, E. W.; Kang, D.; Frisbie, C. D.; Lorkovic, I. M.; Wrighton, M. S. Photosensitive Self-Assembled Monolayers on Gold: Photochemistry of Surface-Confined Aryl Azide and Cyclopentadienylmanganese Tricarbonyl. *J. Am. Chem. Soc.* **1994**, *116*, 4395−4404. (b) Servinis, L.; Henderson, L. C.; Gengenbach, T. R.; Kafi, A. A.; Huson, M. G.; Fox, B. L. Surface functionalization of unsized carbon fiber using nitrenes derived from organic azides. *Carbon* **2013**, *54*, 378−388.

(25) (a) Ciampi, S.; Böcking, T.; Kilian, K. A.; James, M.; Harper, J. B.; Gooding, J. J. Functionalization of Acetylene-Terminated Monolayers on Si(100) Surfaces: A Click Chemistry Approach. *Langmuir* **2007**, *23*, 9320−9329. (b) Mukherjee, S.; Das, M.; Manna, A.; Krishna, R.; Das, S. Newly designed 1,2,3-triazole functionalized covalent triazine frameworks with exceptionally high uptake capacity for both CO2 and H2. *J. Mater. Chem. A* **2019**, *7*, 1055−1068.

(26) Cao, X.; Coulter, S. K.; Ellison, M. D.; Liu, H.; Liu, J.; Hamers, R. J. Bonding of Nitrogen-Containing Organic Molecules to the Silicon(001) Surface: The Role of Aromaticity. *J. Phys. Chem. B* **2001**, *105*, 3759−3768.

(27) Saunders, T. F.; Levy, M. F.; Serino, J. F. Mechanism of the tertiary amine-catalyzed dicyandiamide cure of epoxy resins. *J. Polym. Sci., Part A: Polym. Chem.* **1967**, *5*, 1609−1617.

(28) Gilbert, M. D.; Schneider, N. S.; MacKnight, W. J. Mechanism of the dicyandiamide/epoxide reaction. *Macromolecules* **1991**, *24*, 360−369.

(29) Wu, F.; Zhou, X.; Yu, X. Reaction mechanism, cure behavior and properties of a multifunctional epoxy resin, TGDDM, with latent curing agent dicyandiamide. *RSC Adv.* **2018**, *8*, 8248−8258.

(30) Hong, S.-G.; Kuo, C.-W. The curing behavior of the epoxy/dicyandiamide (DICY)/2- methylimidazole system with intercalated clays. *e-Polym.* **2008**, *8*, 134.

(31) Fedtke, M.; Domaratius, F.; Walter, K.; Pfitzmann, A. Curing of epoxy resins with dicyandiamide. *Polym. Bull.* **1993**, *31*, 429−435.

(32) Zhou, T.; Gu, M.; Jin, Y.; Wang, J. Mechanism and Kinetics of Epoxy-Imidazole Cure Studied with Two Kinetic Methods. *Polym. J.* **2005**, *37*, 833−840.

(33) Perrin, F.-X.; Nguyen, T. M. H.; Vernet, J.-L. Kinetic Analysis of Isothermal and Nonisothermal Epoxy-Amine Cures by Model-Free Isoconversional Methods. *Macromol. Chem. Phys.* **2007**, *208*, 718−729.

(34) Vyazovkin, S.; Sbirrazzuoli, N. Mechanism and Kinetics of Epoxy−Amine Cure Studied by Differential Scanning Calorimetry. *Macromolecules* **1996**, *29*, 1867−1873.

(35) Santiago, D.; Guzmán, D.; Ramis, X.; Ferrando, F.; Serra, À. New Epoxy Thermosets Derived from Clove Oil Prepared by Epoxy-Amine Curing. *Polymers* **2019**, *12*, 44.

(36) (a) Munz, M.; Sturm, H.; Schulz, E.; Hinrichsen, G. The scanning force microscope as a tool for the detection of local mechanical properties within the interphase of fibre reinforced polymers. *Composites, Part A* **1998**, *29*, 1251−1259. (b) Zhao, F.; Huang, Y.; Liu, L.; Bai, Y.; Xu, L. Formation of a carbon fiber/polyhedral oligomeric silsesquioxane/carbon nanotube hybrid reinforcement and its effect on the interfacial properties of carbon fiber/epoxy composites. *Carbon* **2011**, *49*, 2624−2632.

(37) Wen, Z.; Xu, C.; Qian, X.; Zhang, Y.; Wang, X.; Song, S.; Dai, M.; Zhang, C. A two-step carbon fiber surface treatment and its effect on the interfacial properties of CF/EP composites: The electrochemical oxidation followed by grafting of silane coupling agent. *Appl. Surf. Sci.* **2019**, *486*, 546−554.

(38) Ma, L.; Zhang, J.; Teng, C. Covalent functionalization of aramid fibers with zinc oxide nano-interphase for improved UV resistance and interfacial strength in composites. *Compos. Sci. Technol.* **2020**, *188*, 107996.

(39) Yang, L.; Han, P.; Gu, Z. Grafting of a novel hyperbranched polymer onto carbon fiber for interfaical enhancement of carbon fiber reinforced epoxy composites. *Mater. Des.* **2021**, *200*, 109456.

(40) Dharmasiri, B.; Randall, J. D.; Stanfield, M. K.; Ying, Y.; Andersson, G. G.; Nepal, D.; Hayne, D. J.; Henderson, L. C. Using surface grafted poly(acrylamide) to simultaneously enhance the tensile strength, tensile modulus, and interfacial adhesion of carbon fibres in epoxy composites. *Carbon* **2022**, *186*, 367−379.

(41) Wang, S.; Yang, Y.; Mu, Y.; Shi, J.; Cong, X.; Luan, J.; Wang, G. Synergy of electrochemical grafting and crosslinkable crystalline sizing agent to enhance the interfacial strength of carbon fiber/PEEK composites. *Compos. Sci. Technol.* **2021**, *203*, 108562.